JES Focus Issue on Semiconductor Electrochemistry and Photoelectrochemistry in Honor of Krishnan Rajeshwar

Anodic Formation of Nanoporous Indium Phosphide in KOH Electrolytes: Effects of Temperature and Concentration

Nathan Quill,[1] D. Noel Buckley,[1,*] Colm O'Dwyer,[2,3,4,] and Robert P. Lynch[1,**,z]**

[1]*Department of Physics and Bernal Institute, University of Limerick, Limerick, Ireland*
[2]*School of Chemistry, University College Cork, Cork, Ireland*
[3]*Micro-Nano Systems Centre, Tyndall National Institute, Cork, Ireland*
[4]*Environmental Research Institute, University College Cork, Cork, Ireland*

Anodization of n-InP electrodes was carried out over a range of temperatures and KOH concentrations. Scanning electron microscopy showed <111>A aligned pore growth with pore width decreasing as the temperature was increased. This variation is explained in terms of the relative rates of electrochemical reaction and hole diffusion and supports the three-step model proposed earlier. As temperature is increased, both the areal density and width of surface pits decrease resulting in a large increase in the current density through the pits. This explains an observed decrease in porous layer thickness: pits sustain mass transport at the necessary rate for a shorter time before precipitation of etch products blocks the pores. As the concentration of KOH is increased, both pore width and layer thickness decrease to minima at ∼9 mol dm^{-3} after which they again increase. This variation of pore width is also explained by the three-step model and the variation in layer thickness is explained by mass transport effects. Layer porosity follows a similar trend to pore width, further supporting the three-step model. A transition from porous layer formation to planar etching is observed below 2 mol dm^{-3} KOH, and this is also explained by the three-step model.

 [DOI: 10.1149/2.0131905jes]

Manuscript submitted October 17, 2018; revised manuscript received December 20, 2018. Published January 12, 2019. This was Paper 2201 presented at the Honolulu, Hawaii, Meeting of the Society, October 7–12, 2012. *This paper is part of the JES Focus Issue on Semiconductor Electrochemistry and Photoelectrochemistry in Honor of Krishnan Rajeshwar.*

Anodic etching often leads to the formation of porous structures in many materials and can be technologically important in nanofabrication processes. In semiconductors, localized etching can occur, leading to selective removal of material to form a skeletal structure that encompasses a network of pores. Si, SiC, Ge, Ge/Si alloys, and various II-VI and III-V compounds (including InP) can be made porous in such a manner.[1–18]

The morphologies of these pores vary in orientation, frequency of branching, type of infilling and extent of the porous structure. For instance, porous layers form in GaP anodized in aqueous H_2SO_4 solution by the growth of almost hemispherical domains of pores into continuous porous layers.[19] Such domains form due to the radial propagation of their pores from pits in the electrode surface. However, pore propagation can also occur along crystallographic directions and changing the electrode potential can change the propagation direction of these pores. Similar variations in pore morphology are observed in InP and GaAs. In one of the first observations of porous InP formation, pores with triangular cross sections were reported to form along <111> directions when (111)A-oriented n-InP was anodized in the dark in aqueous HCl via an array of periodic holes in a Si mask.[20] Similar pores in both GaAs and InP anodized in HCl[21] have been observed to propagate along the <111>A directions. At higher potentials, propagation of such pores deviates from the crystallographic directions[6,22] and toward the direction of the source of current[23,24] and switching between high and low potential facilitates real-time alternation between these two regimes of "crystallographically-oriented" (CO) and "current-line-oriented" (CLO) pore propagation.[6,25]

The variety of pore morphologies that can be obtained under different conditions has led to the development of a number of models for pore formation in semiconductors.[2,23,26–37] It is generally accepted that pore propagation in highly doped n-type semiconductors is controlled by hole generation under the influence of a high electric field due to the small radius of curvature at the pore tip. Zhang[35] modeled the relationship between pore-tip shape and electric field in silicon and showed that the electric field at the surface is sufficiently enhanced by the curvature at pore-tips to enable substantial tunneling of carriers. This results in significant etching occurring only at pore-tips, allowing continued propagation of these tips into the substrate.

Both chemical and electrochemical etching[38–41] of III-V semiconductors show preferential etching of {111}B planes (i.e. group-V-terminated planes). The slowest-etching plane is usually {111}A and so these facets are revealed during etching of InP,[42,43] GaAs[44–46] and GaP.[47] Due to the differing etch rates of crystal planes, the formation of tetrahedral etch pits (seen as dove-tailed and v-groove voids, respectively in (011) and (01$\bar{1}$) cross sections) is observed on the (100) surface of III-V semiconductors.[1,2,38,43,44]

We have previously shown that anodization of an n-InP electrode in >2 mol dm^{-3} KOH results in the formation of a nanoporous InP layer[3,48–51] of finite thickness.[52–56] Further investigation showed that the porous region is capped by a thin layer (20–40 nm, depending on the conditions) close to the surface that appears to be unmodified. The fact that a porous region can form within the substrate by electrochemical oxidation despite this dense InP layer is explained by the presence of a relatively low areal density (typically ∼10^7 cm^{-2}) of localized channels through the layer. Evidence for the existence of these channels was obtained from both AFM and SEM examination of the surface of electrodes after anodization.[4] It is assumed that both the porous layer and the channels through the near-surface layer are filled with electrolyte, which connects the porous structure with the bulk electrolyte. This enables ionic current to flow and electrochemical oxidation of InP to proceed, providing a mechanism by which the porous layer can grow. The channels within the near-surface layer can thus be seen to play a critical role in the formation of the nanoporous structure.

When anodization is terminated in the early stages, before a continuous porous layer has developed, well-defined porous regions are clearly visible in SEM images of cleaved (01$\bar{1}$) cross sections (i.e. parallel to the secondary flat of the InP wafer).[1,2,4,57,58] This shows that individual, isolated porous domains form in the early stages of

*Electrochemical Society Fellow.
**Electrochemical Society Member.
[z]E-mail: Robert.Lynch@ul.ie

anodization. We have shown that each such domain is separated from the surface by a thin non-porous layer of dense InP[1–4] and is connected to the electrolyte by a single pit which penetrates this near-surface layer. The $(01\bar{1})$-plane cross-sections through these domains are triangular in shape. SEM images of cleaved (011) cross-sections (i.e. parallel to the primary flat of the InP wafer), on the other hand, show quadrilateral porous regions with the shape of isosceles trapezoids. Careful consideration of these cross-sections suggests that all pores propagate only along the four <111>A directions.[1,59,60] This is not unexpected since the fastest etching planes in InP are generally found to be {111}B, i.e. the direction of propagation of the etch front is <111>A. It can be shown[1,54] that such pore propagation from a point on the surface will lead to a porous domain with the shape of a truncated tetrahedron having a triangular cross-section in $(01\bar{1})$ planes and an isosceles trapezoidal cross-section in (011) planes. A comprehensive description of these structures and their formation is given in one of our previous publications.[1]

The formation of crystallographically oriented (CO) <111>A pores suggests that etching is controlled by the relative rates of the surface reactions at different facets and any satisfactory model of electrochemical pore formation must explain how this can occur even though the rate-determining process (hole generation) occurs only at pore tips. To reconcile these requirements, we have proposed[2,61] a three-step model. The three steps are (1) hole generation at pore tips, (2) hole diffusion and (3) electrochemical oxidation of the semiconductor to form etch products, as shown schematically in Fig. 1. These steps and the mechanism by which they lead to preferential pore propagation along <111>A directions are briefly described below. A comprehensive description of the mechanism is given in a previous publication.[2]

Step 1 is the generation of holes at pore tips. This is rate-determining and occurs under the influence of a high electric field due to the small radius of curvature at the pore tip.[31,35] If each hole formed were to be immediately consumed in an electrochemical reaction, then the resulting etching would be confined to a very small area at the pore tip. Step 2 is hole diffusion. Holes may diffuse parallel to the surface of the semiconductor and so the electrochemical etching reaction may occur some distance from the pore tip where the holes are created. As discussed below, this may lead to CO pore formation. Such diffusion of holes from their points of generation to the points where etching ultimately occurs has been reported[46,62] for photoanodic etching of n-type III-V semiconductors where etching was observed to extend beyond the illuminated region.

Step 3 is the actual electrochemical reaction itself. While the detailed chemistry and mechanism of this have not yet been elucidated, it involves oxidation of InP to indium and phosphorus species dissolved in the electrolyte within a pore. The kinetics of Step 3 do not determine the overall etch rate of a pore: this is determined by the rate of generation of holes at the pore tip (Step 1). However, competition in kinetics[46,62,63] between hole diffusion (Step 2) and electrochemical reaction (Step 3) is the principal factor determining the average diffusion distance of holes. If the kinetics of Step 3 (oxidation reaction) are slow relative to Step 2 (diffusion), then holes can diffuse a significant distance before being annihilated in the oxidation reaction. Then etching can occur at preferred crystallographic sites, such as phosphorus dangling bonds in InP, within a zone in the vicinity of the pore tip and will lead to pore propagation in preferential directions. On the other hand, if the kinetics of Step 3 were fast relative to Step 2, the diffusion distance of holes would be short as they would be annihilated in the oxidation reaction close to where they were created. In that case, etching would occur close to the site of hole generation rather than at preferred crystallographic sites and so there would then be no preferred crystal direction for pore propagation.

Thus, if Step 3 (oxidation reaction) is sufficiently fast that Step 1 (hole generation) is rate-determining but sufficiently slow in comparison with Step 2 (diffusion), such that holes can diffuse a significant distance, then preferential etching of {111}B faces can occur. This will eventually reveal the slowest etching crystal facets – the {111}A facets – to form a pyramidal shape with its apex as the pore tip, as shown in Fig. 1b. Etching of {111}A planes one monolayer at a time, then leads to the propagation of pores along <111>A directions.

We have previously proposed[2,6,61] that this model can also explain the variation in porous layer characteristics under different formation conditions. In this paper, we describe anodic etching experiments on n-InP in aqueous KOH under a variety of conditions of temperature and KOH concentration and present a comprehensive analysis of the results in terms of the three-step model.

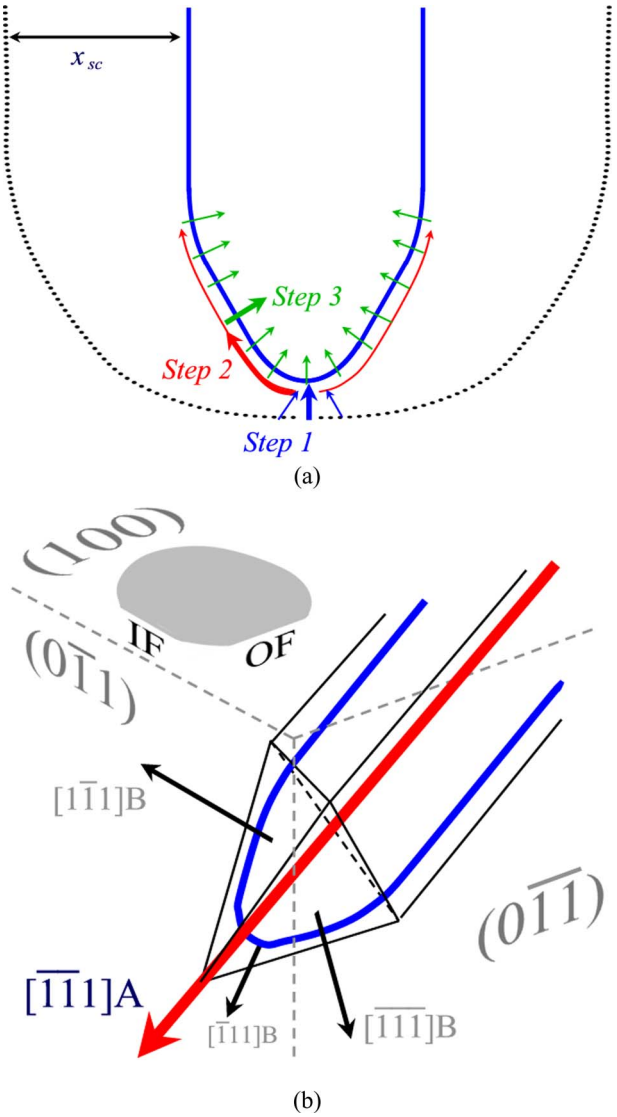

Figure 1. Schematic representations (not to scale) of (a) a pore near its tip showing the three steps of the model of competitive kinetics – (Step 1) hole generation at pore tips by tunnelling of carriers (holes) across the depletion layer (shaded region), where the its width, x_{sc}, is thinnest; (Step 2) hole diffusion near the surface; and (Step 3) electrochemical oxidation of the semiconductor to form etch products – (b) a pore formed by the etching mechanism in (a). The idealized shape with three {111}A internal facets is represented by black lines (▬). The actual pore, represented by blue lines (▬), will have finite radius of curvature at the tip and will generally have rounded pore walls. The orientation of the primary (OF; dovetail-etch; $(0\bar{1}\bar{1})$) and secondary (IF; V-etch; $(0\bar{1}1)$) standard flats and the (100) electrode surface are shown for reference, where the <111>A oriented pore is in the $[\bar{1}\bar{1}\bar{1}]$A direction (Reproduced from Ref. 2 with permission from the PCCP Owner Societies).

Experimental

The wafers used in our studies were generally monocrystalline, sulfur-doped, n-type indium phosphide (n-InP) grown by the liquid-encapsulated Czochralski (LEC) method and supplied by Sumitomo Electric. They were polished on one side and had a surface orientation of (100) and a carrier concentration in the range 3–6 × 10^{18} cm^{-3}. Crystallographic orientation was indicated by primary and secondary flats marking the natural {011} cleavage planes of the wafer according to the European/Japanese system. The manufacturer identified these planes from the 'dovetail' and 'V-groove' etch patterns revealed by a standard wet chemical etch. Thus, the primary flat was chosen so that the {111} plane intermediate in direction between it and the (100) surface plane is a {111}A plane, i.e. In terminated.

To fabricate working electrodes, wafers were cleaved into coupons (typically ~5 mm square) along (011) and (01$\bar{1}$) cleavage planes noting their orientation, i.e. parallel to the primary (OF; dovetail-etch; (0$\bar{1}\bar{1}$)) and secondary (IF; V-etch; (0$\bar{1}$1)) standard flats, respectively, (see Fig. 1b).[1] Ohmic contact was made by alloying indium to the back of a coupon; the back and the cleaved edges were then isolated from the electrolyte by means of a suitable varnish. Prior to immersion in the electrolyte, the working electrode was immersed in a piranha etchant (3:1:1 H_2SO_4:H_2O_2:H_2O) for 4 minutes and then rinsed with deionized water.

Anodization was carried out in aqueous KOH electrolytes in the absence of light using a linear potential sweep at 2.5 mV s^{-1}. A conventional three-electrode cell configuration was used, employing a platinum counter electrode and a saturated calomel electrode (SCE) to which all potentials are referenced. Temperature control was enabled by the use of a jacketed cell and a thermostatic water bath. A CH Instruments Model 650A Electrochemical Workstation interfaced to a Personal Computer (PC) was employed for cell parameter control and for data acquisition.

Electrode surfaces, i.e. (100), and cleaved (011) and (01$\bar{1}$) cross sections of electrodes were examined using either an Hitachi S-4800 or a JEOL JSM-6400F field-emission scanning electron microscope (FE SEM) operating at 5 kV, unless otherwise stated.

Results

Effect of temperature on pore width.—Anodization of n-InP samples by linear potential sweep (LPS) was carried out at a range of temperatures in 9 mol dm^{-3} KOH at a scan rate of 2.5 mV s^{-1}. The resulting linear sweep voltammograms (LSVs) are shown in Fig. 2a. At 10°C the LSV exhibits two current peaks: P_1 at the lower potential and P_2 at the higher potential. As the temperature is increased, these two peaks occur closer together until eventually, at 40°C and above, only a single peak is observed. In all samples, the current density eventually decreases to negligible values indicating the cessation of porous layer growth. The total charge passed (area under curve – Fig. 2b) generally decreases with temperature. The variation in LSVs with temperature will be discussed later but it is first necessary to consider the results of cross-sectional and surface microscopy on anodized electrodes.

SEM micrographs of (011) cross sections of electrodes which have undergone LPS at 10°C and 40°C, respectively, are shown in Figs. 3a, 3b. Typical <111>A aligned pore growth[1,2] is seen in both samples. Clearly, a thinner porous layer is formed at the higher temperature. Figs. 3c, 3d show corresponding higher-magnification images. Narrower pores are seen at the higher temperature. Pore widths measured from micrographs such as these are plotted against anodization temperature in Fig. 4 and it is seen that the average pore width decreases as the temperature is increased.

The variation of pore width with temperature can be explained by the three-step model as being primarily due to variation in the rate of the electrochemical etching reaction.[2,6] Assuming that holes are supplied preferentially to a region of high curvature at a pore tip due to the enhanced electric field in that region,[35] then there is a characteristic diameter for this pore tip; i.e. there exists a characteristic region at the pore tip where carriers can transfer across the depletion layer and etching can take place.[28,35] If holes which arrive at the pore tip are instantly annihilated in an electrochemical reaction, the pore width would be completely determined by the width of this region. However, if the holes have some time to diffuse laterally at the electrode-electrolyte interface before being removed electrochemically, etching would be less spatially confined resulting in wider pores. The pore width would then be determined by a combination of the electric-field distribution at the pore tip, the kinetics of the electrochemical reaction and the rate of hole diffusion. At higher temperatures, the rate of the electrochemical reaction (rate of consumption of holes) is expected to be higher and so holes have less time to diffuse at the interface. Consequently, the effective diffusion length is shorter, leading to more spatially confined etching.

An alternative explanation that narrower pores result from the shorter etching times associated with thinner layers is unlikely because it is known that etching occurs only at the pore tips as evidenced by the lack of variation in pore width from top to bottom of a layer.[2]

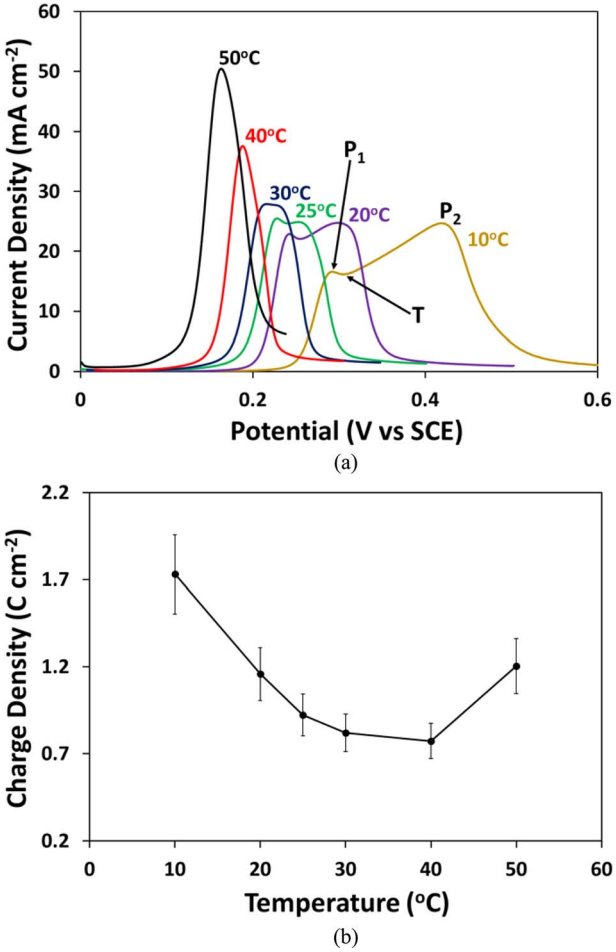

Figure 2. (a) LSVs of InP at 2.5 mV s^{-1} in 9 mol dm^{-3} KOH at various temperatures. The first current peak (P_1), the second current peak (P_2) and the through in current (T) after P_1 are all labelled on the LSV performed at 10°C; (b) total charge passed (area under curves in (a)) plotted against temperature. The standard uncertainty for each data point, primarily from the measurement of electrode area, is shown as error bars. The increase at 50°C appears to be an experimental artifact due to delamination of the insulating varnish.

Effect of temperature on surface pitting and layer thickness.—The surfaces of electrodes anodized as in Fig. 2 were examined by SEM. Fig. 5 shows SEM images of the surface of an electrode anodized at 20°C. The image in Fig. 5a clearly shows scattered etch pits on the surface. The image in Fig. 5b shows a higher magnification image of

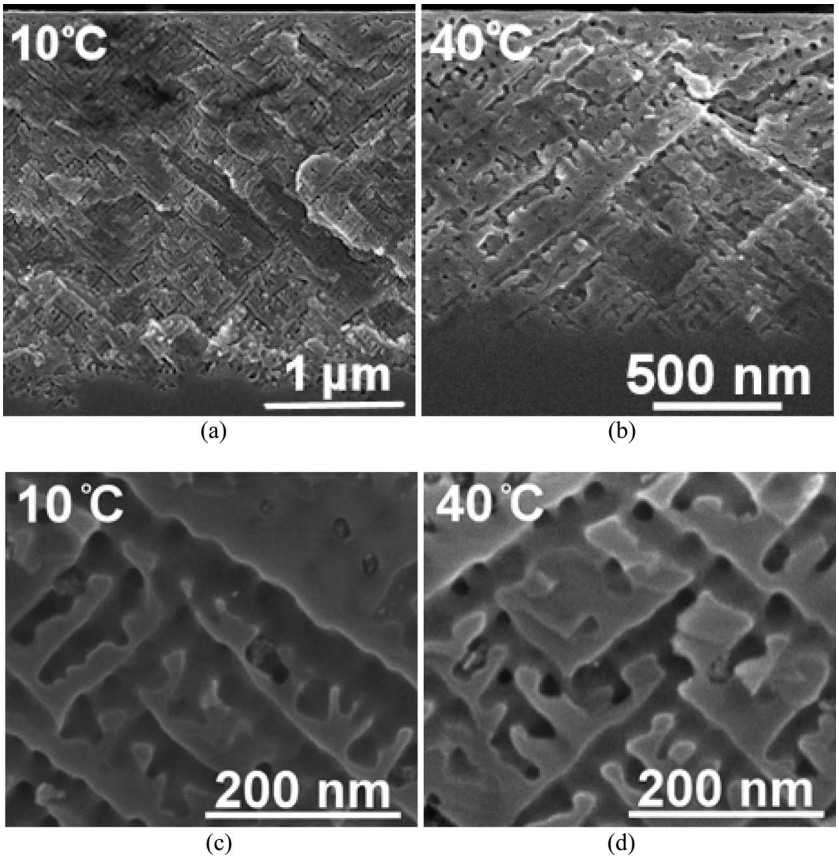

Figure 3. SEM micrographs of (011) cross-sections of InP electrodes after a linear potential sweep in 9 mol dm^{-3} KOH as in Fig. 2. Images (a) and (b) show the porous layers formed at 10°C and 40°C, respectively; (c) and (d) are corresponding higher magnification views showing individual pores.

some typical pits. The average areal density of pits was estimated from images such as Fig. 5a and the average pit width was estimated from images such as Fig. 5b. Similar images were obtained for electrodes subjected to LPS at other temperatures and the areal densities and widths of pits were measured. The resulting plots against temperature are shown in Fig. 6. It is clear from Fig. 6a that the areal density of pits decreases rapidly with increasing temperature. Pit width also decreases with increasing temperature (Fig. 6b), a trend similar to that observed in Fig. 4 for pore width.

The rapid decrease in pit density (Fig. 6a), and the increase in current density (Fig. 2a) indicates that each pit must carry an increased current as temperature is increased. The average current density

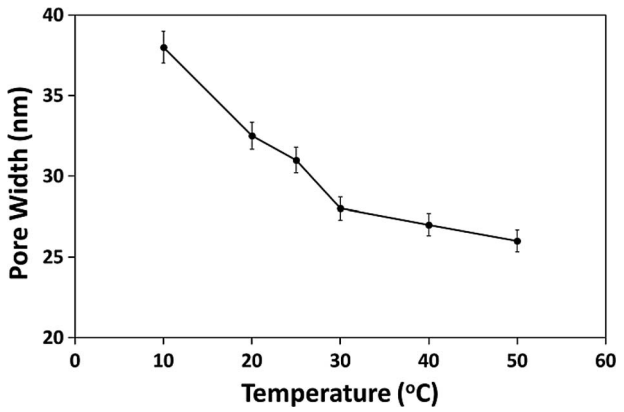

Figure 4. Plot of pore width against temperature for InP electrodes subjected to LPSs at different temperatures in 9 mol dm^{-3} KOH as in Fig. 2. The standard uncertainty in the measurement of each data point is shown as error bars, as is the case with all data plots.

J_{pit} in a pit is

$$J_{pit} = \frac{J}{\pi\sigma(d/2)^2} \quad [1]$$

where d is the pit diameter, σ is the areal density of pits and J is the current density at the electrode. The values of J_{pit} calculated (using the maximum current peak of each LSV in Fig. 2a) from Equation 1 are plotted against temperature in Fig. 7 for the samples anodized as in Fig. 2a. Clearly, the peak current density through a pit increases enormously as temperature is increased, from 12 A cm^{-2} at 20°C to 310 A cm^{-2} at 50°C.

The variation in the density of surface pits and resulting variation in pit current are a key factor in explaining the variation of layer thickness with temperature. Fig. 8 shows a plot of layer thickness, obtained from SEM cross-sections such as those in Fig. 3a, against anodization temperature; it is clear that the layer thickness decreases as the temperature is increased. This may be explained as follows. The rate of formation of etch products (indium and phosphorous species) within a porous layer is, of course, proportional to the current. All of this current flows through the pits connecting the porous layer to the bulk electrolyte. Likewise, all etch products must either remain in the electrolyte within the pores or be transported out through the pits. Thus, in order for a porous layer to continue to grow, the etch products must be transported out through the pits at the rate at which they are formed; otherwise the electrolyte in the pores will become saturated and etch products will precipitate as, for example, indium oxide.[55] Thus, the pit current is a measure of the rate of mass transport through a pit that needs to be sustained in order for pore growth to continue. Clearly, when the current density is high, the pit will no longer be able to sustain mass transport at a sufficient rate, etch products will begin to precipitate in the pores and etching will eventually terminate.

Thus, the large increase in pit current density (Fig. 7) explains the observed decrease in layer thickness (Fig. 8) and shorter etch time (Fig. 2a) as temperature is increased. As the pit current and the

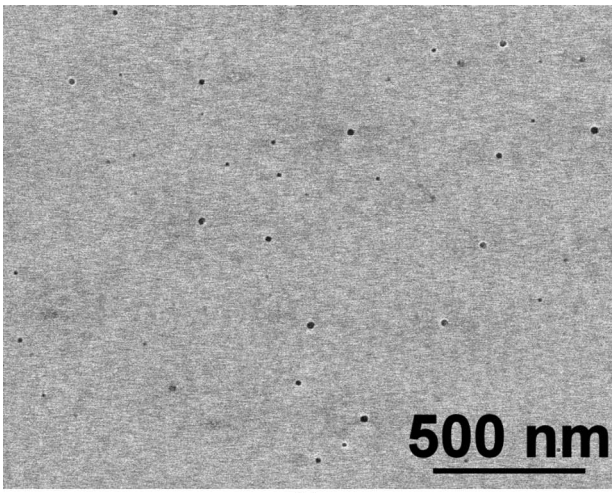

(a)

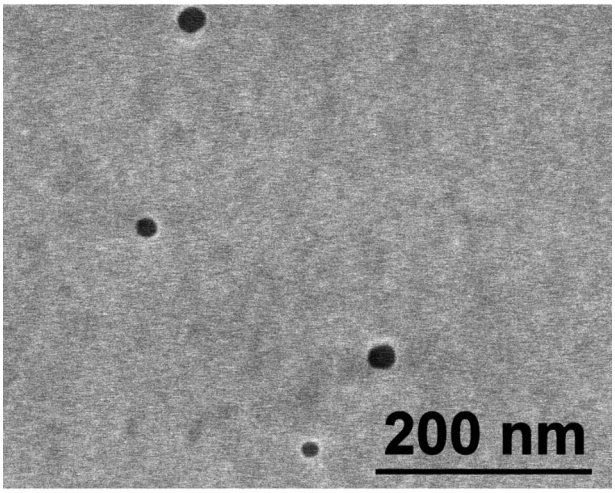

(b)

Figure 5. SEM micrographs of the (100) surface of an InP electrode after a linear potential sweep in 9 mol dm^{-3} KOH at 20°C as in Fig. 2. Pits in the surface can be clearly seen both at low magnification (a) and high magnification (b).

corresponding rate of formation of etch products per pit increases, pits are no longer able to sustain mass transport at the necessary rate, precipitation of etch products begins to block the pores and layer growth terminates. Significant oxide deposits are often observed within the pores of layers whose growth has ceased.[52,55] The earlier termination of porous layer formation at higher temperatures may be further assisted by the narrower pores formed as temperature is increased. The narrower pores are expected to be more susceptible to clogging by oxide precipitates and this would cause porous layer formation to terminate sooner.

The variation of layer thickness with temperature (Fig. 8) shows a very similar trend to that of pore width (Fig. 4) and pit width (Fig. 6b). These relationships are shown more clearly in Fig. 9 where both pore width and pit width are plotted against layer thickness. It is possible[2,61] that the mechanism that controls pit width is to some degree similar to the mechanism which controls pore width and this would explain the correlation between them. Consequently, layer thickness is expected to be correlated with pore width since, as explained above, layer thickness is correlated with pit width.

The rapid decrease in surface pit density with increasing temperature (Fig. 6a) may be explained as follows. Surface pits form at defect sites on the InP surface at which the potential required for etching, E_i, is lower than average for the surface. This can occur, for

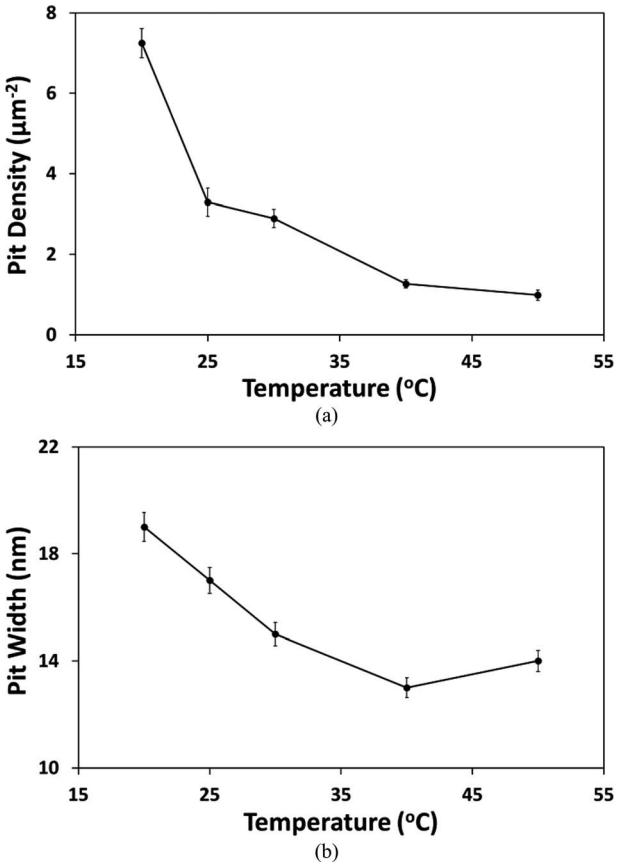

Figure 6. (a) Areal density and (b) width of surface pits plotted against anodization temperature for InP electrodes subjected to LPSs at different temperatures in 9 mol dm^{-3} KOH as in Fig. 2.

example, where there are variations in the energy levels of surface states (due to defects and surface ledges) or variations in the space charge layer thickness (perhaps due to a local perturbation of the doping density).[64,65] Different types of surface defects have different values of E_i and the earliest pits formed will be at sites with the lowest values of E_i. Each pit leads to a porous domain and, as the domain expands, it blocks the formation of etch pits in that region because the entire domain, including the surface above it, becomes depleted of carriers (with the exception of the pore tips).[61] Essentially

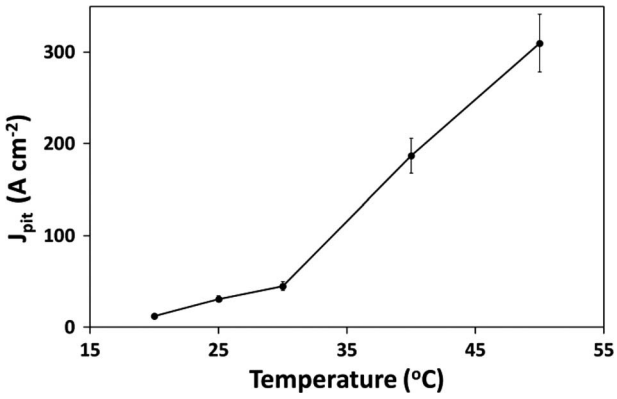

Figure 7. Plot of the peak current density through a surface pit against temperature for InP electrodes subjected to LPSs at different temperatures in 9 mol dm^{-3} KOH as in Fig. 2. Although etching occurs at many points (pore tips) just below the semiconductor surface, all of the mass transport must occur through tiny surface pits.

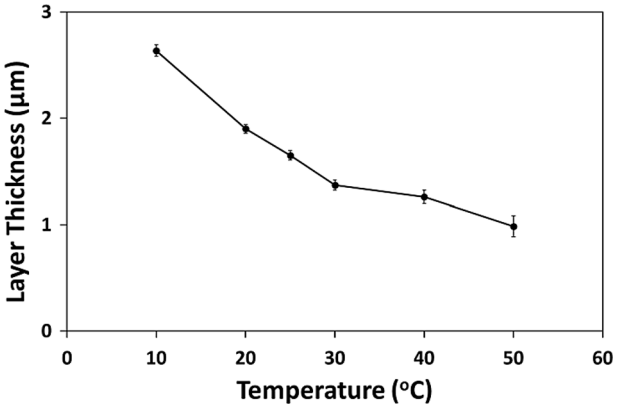

Figure 8. Plot of layer thickness against temperature for InP electrodes subjected to LPSs at different temperatures in 9 mol dm^{-3} KOH as in Fig. 2.

then, there is competition between increasing potential, which enables pitting at sites with increasing values of E_i, and current-related expansion of porous domains which prevents pitting in the vicinity of existing porous domains; the rate of increase of potential (scan rate) is constant for all experiments but the current is temperature-dependent. As can be seen from Fig. 2a, at higher temperatures electrodes reach higher current densities at lower potentials. Consequently, the porous domains expand more rapidly at higher temperatures and this leads to a lower density of pits.

This raises the question of why the current density is higher at higher temperatures. As we have seen (Fig. 4) pores are narrower at higher temperatures. For any given current per pore tip, the rate of advance will be faster for a narrower pore. Consequently, the rate of formation of branched pores will be higher since the tip must advance some characteristic distance for branching to occur.[2] Thus the number of new pores created per unit time, and consequently the rate of increase of current, is higher at higher temperatures.

Variation of LSVs with temperature.—We can now explain the change in the LSVs in Fig. 2 as temperature is changed. A detailed analysis of how the progression of porous etching in InP in KOH relates to the features of LSVs is given elsewhere.[66]

Each surface pit leads to a porous domain and so, when the areal density of pits is high, domains are numerous and consequently will have grown only to a small size when they merge, i.e. when they begin to restrict each other's lateral growth. Obviously, the layer formed when smaller domains merge is thinner than one formed when larger domains merge. Thus, at low temperatures, peak P_1 in Fig. 2a (which corresponds to domain merging)[66] occurs at a low layer thickness

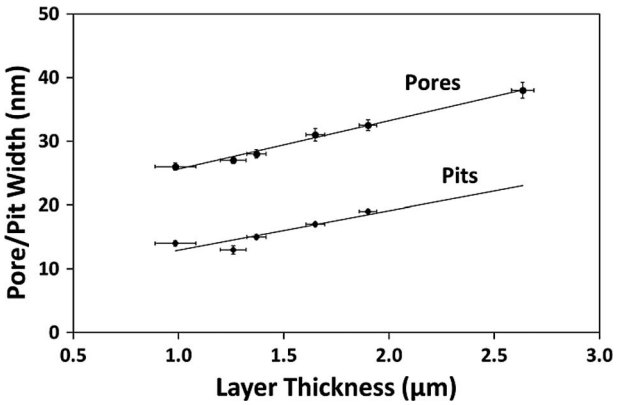

Figure 9. Plot of (a) pore width (-●-) (from Fig. 4) and (b) pit width (-♦-) (from Fig. 6b) against layer thickness (from Fig. 8).

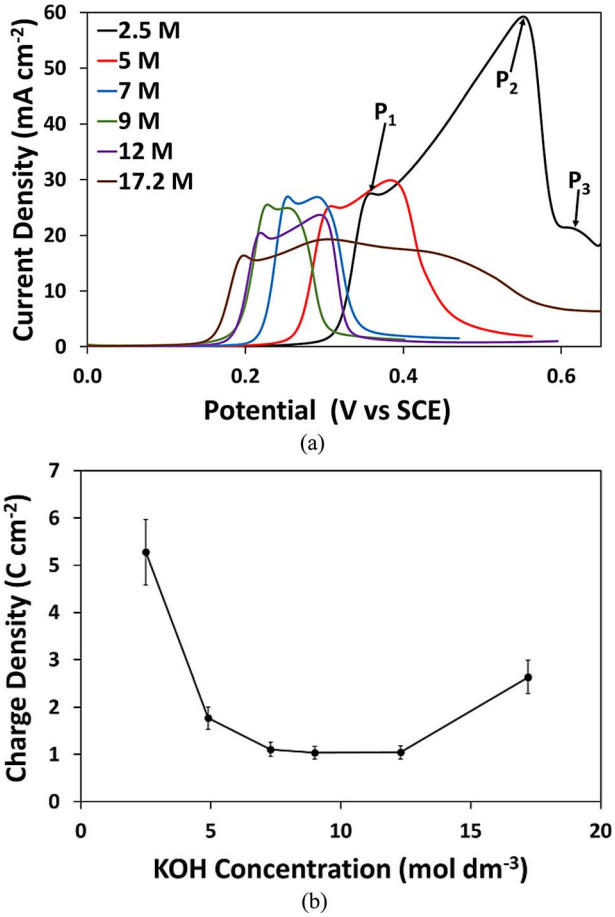

Figure 10. (a) LSVs of InP electrodes anodized in a range of KOH concentrations at 2.5 mV s^{-1} at 25°C. The current peaks P_1 and P_2, as well as the current plateau P_3 are labelled on the LSV at 2.5 mol dm^{-3}. (b) Charge passed (integrated area under curves in (a)) plotted against concentration. The concentration was varied from 2.5 mol dm^{-3} to 17 mol dm^{-3}.

because the density of pits is high (Fig. 6a). However, final layer thickness is high at low temperatures (Fig. 8). Consequently, P_2 in Fig. 2 (which corresponds to cessation of layer growth)[66] occurs at a much greater layer thickness than P_1 (domain merging). At higher temperatures, the density of pits decreases and so the layer thickness at P_1 increases while the final layer thickness (i.e., the layer thickness at P_2) decreases. Consequently, at higher temperatures, the peaks P_1 and P_2 are closer to each other and at sufficiently high temperatures they merge into a single peak.

We have already discussed the higher currents observed at higher temperatures. It is also apparent from Fig. 2a that the onset voltage for pitting is lower at higher temperatures. Although electrochemical reaction is not rate-determining for pore growth, it may be rate-determining for pit initiation. Thus, the rate of pit formation is likely determined by both temperature and potential and consequently pitting begins at a lower potential at higher temperatures.

Effect of KOH concentration on porous layers.—We have previously shown that anodic etching of n-InP in concentrated KOH solutions results in the formation of crystallographically oriented (CO) porous layers.[1,2,4,59] Here we show the results of series of experiments in which n-InP was anodized in KOH solutions over a wide range of concentrations.

Porous layers were formed anodically in n-InP in KOH concentrations ranging from 2.5 to 17 mol dm^{-3} by linear potential sweep (LPS) at 2.5 mV s^{-1} at 25°C. The resulting linear sweep voltammograms (LSVs) are shown in Fig. 10a. Each LSV exhibits two current peaks;

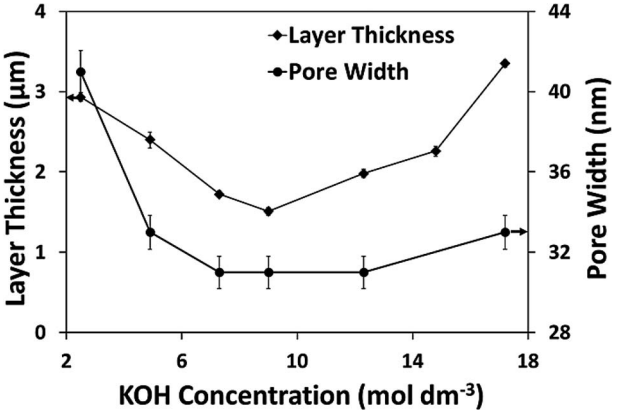

Figure 11. Plots of porous layer thickness (-♦-) and pore width (-●-) against KOH concentration for InP electrodes anodized by LPS at 2.5 mV s^{-1} at 25°C in different concentrations of KOH as in Fig. 10.

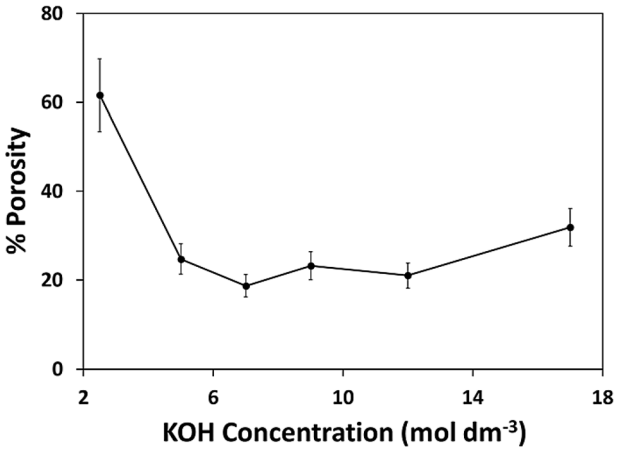

Figure 12. Plot of percentage porosity against KOH concentration for InP electrodes anodized by LPS at 2.5 mV s^{-1} at 25°C in different concentrations of KOH as in Fig. 10.

P_1 (at the lower potential) and P_2 (at the higher potential); there is also a current shoulder, P_3, on the high-potential side of P_2 in some of the LSVs. As the concentration is increased, both peaks generally shift to lower potentials and the currents generally decrease. The charge passed (area under curve – Fig. 10b) exhibits a broad minimum at ~9 mol dm^{-3}; it increases at both higher and lower concentrations.

Pore width and layer thickness measured from micrographs similar to those in Fig. 3 are plotted against KOH concentration in Fig. 11. Both decrease to a minimum as the concentration increases from 2.5 mol dm^{-3} to ~9 mol dm^{-3}. However, the layer thickness increases as the concentration is increased above ~9 mol dm^{-3} and pore width somewhat increases (above ~12 mol dm^{-3}). Thus, pore width and layer thickness appear correlated; this correlation is similar to (but weaker than) that discussed above in the case of temperature variation.

The effect of KOH concentration on pore width can be explained by the three-step model in a manner similar to the effect of temperature discussed above. The effect is due to variation in the rate of the electrochemical etching reaction and consequent variation in the diffusion distance of holes at the InP-electrolyte interface (see Fig. 1a). We postulate that the rate of the electrochemical reaction is lower at lower concentrations, and that it increases as the concentration is increased. Consequently, holes have less time to diffuse laterally before being removed electrochemically and so etching is spatially confined and the average pore width decreases. This would explain the decrease in pore width as the concentration increases from 2.5 mol dm^{-3} to 7 mol dm^{-3}. Above 7 mol dm^{-3}, pore width is relatively constant but appears to increase somewhat above ~12 mol dm^{-3}. This suggests that the rate of the electrochemical reaction reaches a maximum at approximately 9 mol dm^{-3} and decreases somewhat at higher concentrations. Interestingly, reported values for the specific conductivity of KOH[67] show that it reaches a maximum at approximately 7 mol dm^{-3} and decreases with increasing concentration thereafter. This suggests that a decrease in the kinetics of the electrochemical reaction at higher KOH concentrations may be due to a change in the structure of the electrolyte.

As discussed in the case of temperature above, layer thickness is determined by eventual precipitation of etch products which block the pores and cause layer growth to terminate. Thus mass transport of etch products appears to be least favored at intermediate concentrations of KOH. A correlation between layer thickness and pore width was already noted and as previously suggested,[55] thinner pores may be more susceptible to blocking by oxide precipitates leading to a more rapid cessation of porous layer growth at higher temperatures.

The porosity of a layer is d_e/d_m where d_m is the microscopically measured layer thickness and d_e is the equivalent thickness etched given by

$$d_e = \frac{QV_m}{nF}$$

where Q is the charge passed per unit area, V_m is the molar volume of InP, F is the Faraday constant, and n is the number of electrons involved in the anodic reaction (taken to be 8). Values of porosity were calculated from measured values of Q (Fig. 10) and corresponding values of d_m (Fig. 11); results are plotted in Fig. 12. It is clear that the porosity follows a similar trend to the pore width (Fig. 11), initially decreasing with increasing KOH concentration, reaching a minimum and somewhat increasing thereafter. The fact that porosity increases as the pore width increases indicates that the increase in pore width is not being compensated for by a corresponding increase in the pore wall thickness. Thus, the larger pore widths are apparently due to increased etching of pore walls without any significant change in the overall pore spacing (i.e. inter-axial distance between pores). This supports the three-step model as it is consistent with pore broadening due to increased diffusion distance of holes rather than any change in the spacing of pore tips.

The increased separation between P_1 and P_2 in the LSVs (Fig. 10a) at both high and low concentrations can be explained by the corresponding increases in layer thickness (Fig. 11). This is similar to the effect discussed above for temperature. It is also apparent from Fig. 10 that the onset voltage for pitting is lower at higher concentrations of KOH. As mentioned earlier, although the electrochemical reaction is not rate-determining for pore growth, it may be rate-determining for pit initiation. Thus, the rate of pit formation is likely determined by both KOH concentration and potential (as well as temperature) and consequently pitting begins at a lower potential at higher concentrations of KOH.

The transition from porous layer formation to planar etching.— A series of experiments was performed in which n-InP samples were anodized in successively lower concentrations of KOH in order to more closely examine the lower limits of pore formation. Figure 13 shows a series of LSVs of InP in KOH solutions varying from 2.0 to 1.0 mol dm^{-3}. The LPSs were stopped at an upper potential of 0.75 V because previous studies[66] have shown that the etching mechanism changes at higher potentials, resulting in the undercutting and removal of the porous layer. The shape of the LSV at 2.0 mol dm^{-3} KOH is similar to that seen for porous layer formation in Fig. 10a, i.e. current begins to increase at a characteristic potential, and then exhibits two peaks followed by a rapid decrease. In the LSV at 1.9 mol dm^{-3}, the first peak is still discernable, as is the pseudo-linear increase in current typically found between the two peaks; however, no drop in current is seen at higher potentials (i.e. P_2 no longer appears as a peak). At concentrations from 1.7 – 1.2 mol dm^{-3} the LSVs are similar to that at 1.9 mol dm^{-3} but the current gradually decreases and the onset potential drifts to higher values. Below 1.2 mol dm^{-3}, there is a large

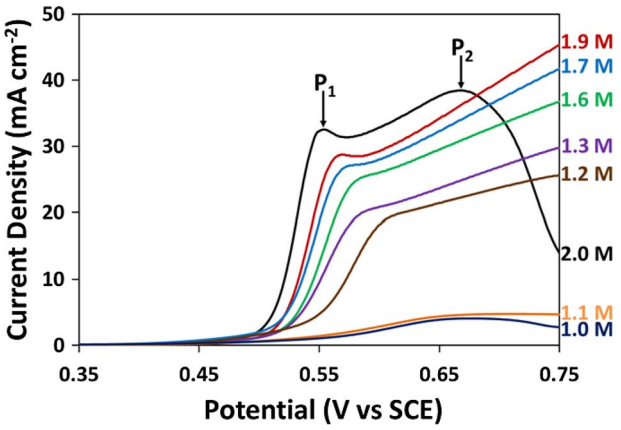

Figure 13. LSVs of InP electrodes anodized in a range of KOH concentrations from 2.0 mol dm^{-3} to 1.0 mol dm^{-3} KOH at a scan rate of 2.5 mV s^{-1}.

reduction in current; there is little further change as the concentration is reduced to 1 mol dm^{-3}.

SEM images of (011) cross-sections of the electrodes anodized as in Fig. 13 are shown in Fig. 14. The transition to porous layer formation with increasing concentration is shown in (c) - (f). The layer (f) obtained in 1.8 mol dm^{-3} KOH is clearly similar to layers obtained at higher concentrations although the dense near-surface layer observed at higher concentrations is not evident. The top surface of the layer is quite smooth and planar suggesting that it is likely the remnants of the original electrode surface. At a concentration of 1.7 mol dm^{-3} (e) the layer thickness is considerably reduced (~0.8 μm) and the surface appears to be rough. The pore size also appears to be somewhat larger. This trend to larger pore sizes and thinner layers as the concentration is decreased is seen to continue at 1.6 mol dm^{-3} (d) and 1.2 mol dm^{-3} (c), until eventually no porous layers are observed at 1.1 mol dm^{-3} (b) or 1.0 mol dm^{-3} (a).

The porous layer thickness and pore width were measured, where possible, from SEM cross sections such as those in Fig. 14 and the results are shown in Table I. At electrolyte concentrations between 1.8 mol dm^{-3} and 1.2 mol dm^{-3}, pore widths are in the approximate range of 50–200 nm with pore walls of less than 10 nm. It is also observed that at these lower concentrations, pores eventually grow into each other. Unlike the structures obtained at higher concentrations, where pore walls act as a barrier to the propagation of other pores,[2] the pore walls in the structures formed at low concentrations can be etched. This unexpected etching also extends to the original electrode surface. This could be due to chemical etching of the porous structure, either by KOH, or more likely, by products of the electrochemical reactions. However, as we will show later, it could also be due to the inherent characteristics of the etching mechanism.

Table I. The variation of layer thickness and pore width with KOH concentration as porous etching transitions to planar etching, corresponding to the LSVs and SEM images presented in Figs. 13 and 14. Note that the InP wafer used for these experiments had a slightly higher carrier concentration than those used for all other experiments presented in this paper. As a result, the pore widths in this table are slightly different from those in Figs. 4, 9 and 11.

KOH Concentration, [KOH] (mol dm^{-3})	Layer Thickness (μm)	Pore Width (nm)
2	2.6	63
1.8	2.2	61
1.7	0.8	67
1.6	0.2	72
1.5	0.8	75
1.4	0.6	78
1.3	0.4	82
1.2	0.4	93

The narrowing of the pore walls (and the related increase in pore width) at lower KOH concentrations continues the general trend observed for the variation of pore width with concentration (see Fig. 11). Due to the uncertainties in layer thickness measurements at these concentrations (see Table I), and also in the coulometry due to the lack of a definitive current drop (i.e., no P_2), the exact porosity is difficult to determine. However, the general observation of increased pore width and decreased pore wall thickness suggests that the trend of increasing porosity, which was observed as concentration is reduced in the range 2.5–9 mol dm^{-3} (Fig. 12), is sustained as concentration is reduced below 2 mol dm^{-3}.

In summary, as the KOH concentration is decreased, pore diameters become wider, pore walls become narrower and porous layer thickness becomes lower until eventually anodization simply results in the formation of a rough surface (i.e., a surface of short and wide pores) at ~1.2 mol dm^{-3} (Fig. 14c). This trend is continued at even lower concentrations until eventually a smooth surface (i.e. planar etching) is achieved at ~1 mol dm^{-3}. It is noted that the etch rate at this concentration is very much lower than that for porous layer formation as evidenced by the low current density in Fig. 13.

The three-step model can also explain the transition from localized etching (porous layer formation) to planar etching. It is suggested that the rapid increase in pore width at low concentrations occurs because the rate of the electrochemical reaction decreases rapidly below 2 mol dm^{-3}. Consequently, holes can diffuse laterally for a significantly greater distance before being removed electrochemically and so etching is less spatially confined. This leads to increasingly wider pores and increasingly narrower pore walls until eventually the pores grow into each other and individual pores become difficult to distinguish (see Fig. 14e). At this point, holes become available at essentially every point on the electrode surface, leading to planar etching. Another consequence of this is the significantly reduced rate of hole supply caused by the reduction in curvature (smoothing) at the electrode surface. This severely limits the rate of the etching reaction as evidenced by the much smaller current density and higher potential required for etching for the 1.1 and 1.0 mol dm^{-3} samples in Fig. 13.

The absence of P_2 in the LSVs below 2 mol dm^{-3} in Fig. 13 can be explained by the absence of a near-surface layer in SEM images of these electrodes in Fig. 14. As previously mentioned, P_2 is due to layer growth cessation caused by mass transport limitations through surface pits. With the near surface layer removed, mass transport through the surface is enhanced and the typical drop in current after P_2 is not observed under these experimental conditions.

Conclusions

Anodization of n-InP electrodes was carried out by linear potential sweep over a range of temperatures from 10°C to 50°C in 9 mol dm^{-3} KOH. SEM micrographs of (011) cross sections of electrodes showed <111>A aligned pore growth with both pore width and layer thickness decreasing as the temperature was increased. The variation of pore width with temperature is explained by the three-step model as being primarily due to variation in the rate of the electrochemical etching reaction. SEM images showed that both the areal density and width of surface pits decrease as temperature is increased. Consequently, there is a large increase in the current density in the pits. This explains the observed decrease in layer thickness: pits are no longer able to sustain mass transport at the necessary rate, and precipitation of etch products begins to block the pores, terminating layer growth.

Each LSV exhibits two current peaks: P_1, corresponding to porous domain merging, and P_2, corresponding to termination of layer growth. As the temperature is increased, the two peaks move closer together and eventually merge, primarily because the final layer thickness decreases. LSVs also show that at higher temperatures electrodes reach higher current densities at lower potentials and porous domains expand more rapidly. We propose that this leads to a lower density of pits because a domain, being depleted of carriers, prevents the

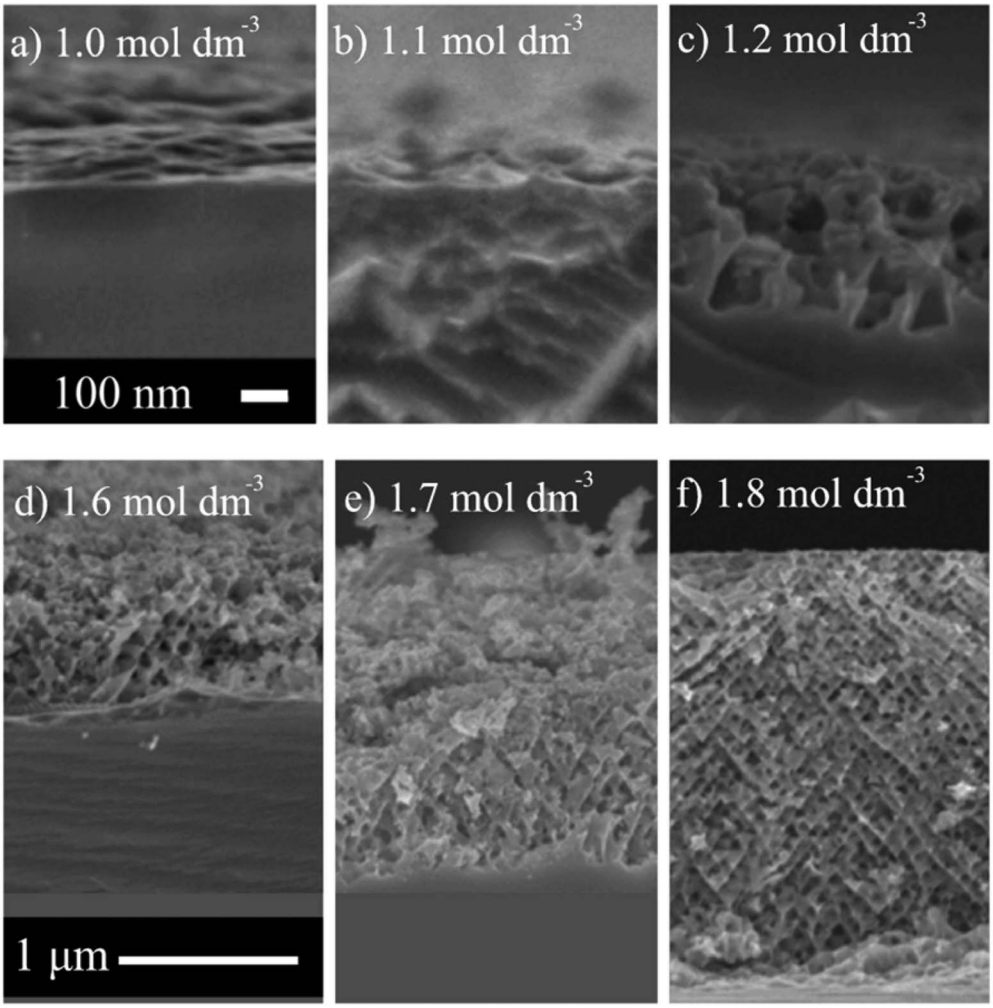

Figure 14. Cross-sectional SEM micrographs of the (011) cleaved planes of InP electrodes anodized by LPS from 0.0 to 0.75 V (SCE) at 2.5 mV s^{-1} in KOH solutions of the concentrations shown.

formation of pits in the surface above it. It is likely that the higher current densities observed occur because the pores are narrower at higher temperatures and so they advance more rapidly leading to more rapid branching and consequently a more rapid increase in the number of pore tips. The onset voltage for pitting is also lower at higher temperatures, suggesting that pit-formation is controlled by an electrochemical reaction which according to the three-step model is faster at higher temperature.

Anodization of n-InP electrodes was also carried out over a range of concentrations from 1.0 to 17 mol dm^{-3} KOH at 25°C. At 2.0 mol dm^{-3} and above, LSVs showed that layers terminated at a finite thickness and SEM cross-sections showed a thin near-surface layer separating the porous layer from the electrolyte. Below 2.0 mol dm^{-3} LSVs did not show a final termination of layer growth (no drop in current) and there was no evidence of a dense near-surface layer in SEM cross-sections. Below ∼1.2 mol dm^{-3}, no porous layer was observed.

SEM micrographs of (011) cross section of electrodes anodized in range of 2.5 to 17 mol dm^{-3} KOH showed that both pore width and layer thickness were at a minimum at ∼9 mol dm^{-3} and increased at concentrations either above or below this. The variation of pore width with temperature is explained by the three-step model as primarily due to variation in the rate of the electrochemical etching reaction. The variation in layer thickness is explained by effects on the mass transport of etch products. Layer porosity follows a similar trend to the pore width. This supports the three-step model as it is consistent with pore broadening due to longer diffusion distance of holes rather than any change in the spacing of pore tips.

Each LSV in the range 2.5–17 mol dm^{-3} KOH exhibits two current peaks, P_1 and P_2, which move farther apart due to increasing layer thickness at concentrations either above or below ∼9 mol dm^{-3}. The onset voltage for pitting is also lower at higher concentrations, suggesting that pit-formation is controlled by an electrochemical reaction that is faster at higher concentrations.

The transition from localized porous etching to planar etching can also be explained by the three-step model. Pores increase in width below ∼7 mol dm^{-3} KOH and at 2 mol dm^{-3}, pore widths of >50 nm are observed. Pore width increases further as concentration is decreased below 2 mol dm^{-3} until at ∼1.1 mol dm^{-3} no porous layer is observed. This rapid increase in pore width suggests that the kinetics of the electrochemical reaction decreases rapidly below 2 mol dm^{-3}. Consequently, holes can diffuse laterally for significantly greater distance before being removed electrochemically and so etching is less spatially confined. This leads to increasingly wider pores and increasingly narrower pore walls until eventually the pores grow into each other leading to planar etching.

Acknowledgments

The support of the Irish Research Council (IRC) and Government of Ireland funding is gratefully acknowledged. R.P. Lynch acknowledges a joint IRC-Marie Skłodowska Curie Fellowship

under grant No. INSPIRE PCOFUND-GA-2008-229520 and Science Foundation Ireland (SFI) National Access Program (NAP) funding (37 and 70) for research at the Tyndall National Institute, Cork. C. O'Dwyer acknowledges support from SFI under contract No. 07/SK/B1232a and IA/14/2581, and under the framework of the INSPIRE programme, funded by the Irish Government's Programme for Research in Third Level Institutions, Cycle 4, National Development Plan 2007–2013.

ORCID

Nathan Quill https://orcid.org/0000-0002-3736-548X
D. Noel Buckley https://orcid.org/0000-0002-3006-8837
Colm O'Dwyer https://orcid.org/0000-0001-7429-015X
Robert P. Lynch https://orcid.org/0000-0003-3547-5711

References

1. R. P. Lynch, C. O'Dwyer, N. Quill, S. Nakahara, S. B. Newcomb, and D. Noel Buckley, *J. Electrochem. Soc.*, **160**, D260 (2013).
2. R. P. Lynch, N. Quill, C. O'Dwyer, S. Nakahara, and D. N. Buckley, *Phys. Chem. Chem. Phys.*, **15**, 15135 (2013).
3. C. O'Dwyer, D. N. Buckley, D. Sutton, and S. B. Newcomb, *J. Electrochem. Soc.*, **153**, G1039 (2006).
4. C. O'Dwyer, D. N. Buckley, D. Sutton, M. Serantoni, and S. B. Newcomb, *J. Electrochem. Soc.*, **154**, H78 (2007).
5. N. Quill, R. P. Lynch, C. O'Dwyer, and D. N. Buckley, *ECS Trans.*, **50**, 377 (2013).
6. N. Quill, R. P. Lynch, C. O'Dwyer, and D. N. Buckley, *ECS Trans.*, **50**, 143 (2013).
7. A. M. Gonçalves, L. Santinacci, A. Eb, C. David, C. Mathieu, M. Herlem, and A. Etcheberry, *phys. stat. sol., A*, **204**, 1286 (2007).
8. A. M. Goncalves, L. Santinacci, A. Eb, I. Gerard, C. Mathieu, and A. Etcheberry, *Electrochem. Solid-State Lett.*, **10**, D35 (2007).
9. M. Schoisswohl, J. L. Cantin, M. Chamarro, H. J. von Bardeleben, T. Morgenstern, E. Bugiel, W. Kissinger, and R. C. Andreu, *Phys. Rev., B*, **52**, 11898 (1995).
10. A. G. Cullis, L. T. Canham, and P. D. J. Calcott, *J. Appl. Phys.*, **82**, 909 (1997).
11. T. Osaka, K. Ogasawara, and S. Nakahara, *J. Electrochem. Soc.*, **144**, 3226 (1997).
12. D. J. Lockwood, P. Schmuki, H. J. Labbé, and J. W. Fraser, *Physica E*, **4**, 102 (1999).
13. S. Langa, J. Carstensen, I. M. Tiginyanu, M. Christophersen, and H. Foll, *Electrochem. Solid-State Lett.*, **4**, G50 (2001).
14. J. J. Kelly and H. G. G. Philipsen, *Curr. Opin. Solid State Mater. Sci.*, **9**, 84 (2005).
15. C. Fang, H. Föll, J. Carstensen, and S. Langa, *phys. stat. sol., A*, **204**, 1292 (2007).
16. C. Fang, H. Föll, and J. Carstensen, *J. Electroanal. Chem.*, **589**, 259 (2006).
17. M. Christophersen, J. Carstensen, S. Rönnebeck, C. Jäger, W. Jäger, and H. Föll, *J. Electrochem. Soc.*, **148**, E267 (2001).
18. P. Schmuki, L. Santinacci, T. Djenizian, and D. J. Lockwood, *phys. stat. sol., A*, **182**, 51 (2000).
19. B. H. Erne, D. Vanmaekelbergh, and J. J. Kelly, *J. Electrochem. Soc.*, **143**, 305 (1996).
20. T. Takizawa, M. Nakahara, E. Kikuno, and S. Arai, *J. Electron. Mater.*, **25**, 657 (1996).
21. S. Langa, J. Carstensen, M. Christophersen, K. Steen, S. Frey, I. M. Tiginyanu, and H. Föll, *J. Electrochem. Soc.*, **152**, C525 (2005).
22. H. Fujikura, A. Liu, A. Hamamatsu, T. Sato, and H. Hasegawa, *Jpn. J. Appl. Phys.*, **39**, 4616 (2000).
23. F. M. Ross, G. Oskam, P. C. Searson, J. M. Macaulay, and J. A. Liddle, *Philos. Mag. A*, **75**, 525 (1997).
24. S. Langa, I. M. Tiginyanu, J. Carstensen, M. Christophersen, and H. Foll, *Electrochem. Solid-State Lett.*, **3**, 514 (2000).
25. H. Tsuchiya, M. Hueppe, T. Djenizian, and P. Schmuki, *Surf. Sci.*, **547**, 268 (2003).
26. M. J. J. Theunissen, *J. Electrochem. Soc.*, **119**, 351 (1972).
27. T. Unagami, *J. Electrochem. Soc.*, **127**, 476 (1980).
28. M. I. J. Beale, J. D. Benjamin, M. J. Uren, N. G. Chew, and A. G. Cullis, *J. Cryst. Growth*, **73**, 622 (1985).
29. V. Lehmann and H. Foll, *J. Electrochem. Soc.*, **137**, 653 (1990).
30. V. Lehmann and U. Gosele, *Appl. Phys. Lett.*, **58**, 856 (1991).
31. X. G. Zhang, *J. Electrochem. Soc.*, **138**, 3750 (1991).
32. R. L. Smith and S. D. Collins, *J. Appl. Phys.*, **71**, R1 (1992).
33. P. Allongue and C. H. de Villeneuve, *Appl. Phys. Lett.*, **67**, 941 (1995).
34. J. Cartensen, M. Christophersen, and H. Foll, *Mat. Sci. Eng., B*, **69–70**, 23 (2000).
35. X. G. Zhang, *J. Electrochem. Soc.*, **151**, C69 (2004).
36. J. N. Chazalviel, R. B. Wehrspohn, and F. Ozanam, *Mat. Sci. Eng., B*, **69–70**, 1 (2000).
37. J.-N. Chazalviel, F. Ozanam, N. Gabouze, S. Fellah, and R. B. Wehrspohn, *J. Electrochem. Soc.*, **149**, C511 (2002).
38. S. N. G. Chu, C. M. Jodlauk, and W. D. Johnston, *J. Electrochem. Soc.*, **130**, 2398 (1983).
39. D. Soltz and L. Cescato, *J. Electrochem. Soc.*, **143**, 2815 (1996).
40. D. N. MacFayden, *J. Electrochem. Soc.*, **130**, 1934 (1983).
41. H. C. Gatos and M. C. Lavine, *J. Electrochem. Soc.*, **107**, 427 (1960).
42. P. H. L. Notten, *J. Electrochem. Soc.*, **138**, 243 (1991).
43. I. E. Vermeir, W. P. Gomes, and P. Van Daele, *J. Electrochem. Soc.*, **142**, 3226 (1995).
44. Y. Tarui, Y. Komiya, and Y. Harada, *J. Electrochem. Soc.*, **118**, 118 (1971).
45. S. Adachi and K. Oe, *J. Electrochem. Soc.*, **130**, 2427 (1983).
46. M. M. Carrabba, N. M. Nguyen, and R. D. Rauh, *J. Electrochem. Soc.*, **134**, 1855 (1987).
47. H. H. Goossens and W. P. Gomes, *J. Electrochem. Soc.*, **138**, 1696 (1991).
48. R. P. Lynch, C. O'Dwyer, D. N. Buckley, D. Sutton, and S. Newcomb, *ECS Trans.*, **2**, 131 (2006).
49. D. N. Buckley, C. O'Dwyer, R. Lynch, and N. Quill, *ECS Trans.*, **35**, 29 (2011).
50. N. Quill, R. P. lynch, C. O'Dwyer, and D. N. Buckley, *ECS Trans.*, **50**, 131 (2013).
51. D. N. Buckley, R. P. Lynch, N. Quill, and C. O'Dwyer, *ECS Trans.*, **69**, 17 (2015).
52. R. P. Lynch, M. Dornhege, P. S. Bodega, H. H. Rotermund, and D. N. Buckley, *ECS Trans.*, **6**, 331 (2007).
53. N. Quill, C. O'Dwyer, R. Lynch, and D. N. Buckley, *ECS Trans.*, **19**, 295 (2009).
54. R. P. Lynch, N. Quill, C. O'Dwyer, and D. N. Buckley, *ECS Trans.*, **50**, 191 (2013).
55. R. P. Lynch, N. Quill, C. O'Dwyer, M. Dornhege, H. H. Rotermund, and D. N. Buckley, *ECS Trans.*, **53**, 65 (2013).
56. N. Quill, R. P. Lynch, C. O'Dwyer, and D. N. Buckley, *ECS Trans.*, **58**, 25 (2013).
57. R. P. Lynch, C. O'Dwyer, D. Sutton, S. B. Newcomb, and D. N. Buckley, *ECS Trans.*, **6**, 355 (2007).
58. N. Quill, C. O'Dwyer, D. N. Buckley, and R. P. Lynch, *ECS Trans.*, **69**, 33 (2015).
59. R. Lynch, C. O'Dwyer, N. Quill, S. Nakahara, S. B. Newcomb, and D. N. Buckley, *ECS Trans.*, **16**, 393 (2008).
60. R. P. Lynch, N. Quill, C. O'Dwyer, S. Nakahara, and D. N. Buckley, *ECS Trans.*, **50**, 319 (2013).
61. N. Quill, L. Green, C. O'Dwyer, D. N. Buckley, and R. P. Lynch, *ECS Trans.*, **75**, 29 (2017).
62. F. W. Ostermayer, P. A. Kohl, and R. M. Lum, *J. Appl. Phys.*, **58**, 4390 (1985).
63. S. W. Benson, *The foundations of chemical kinetics*, p. 66, McGraw-Hill (1960).
64. I. M. Tiginyanu, C. Schwab, J.-J. Grob, B. Prévot, H. L. Hartnagel, A. Vogt, G. Irmer, and J. Monecke, *Appl. Phys. Lett.*, **71**, 3829 (1997).
65. P. Schmuki, L. E. Erickson, D. J. Lockwood, B. F. Mason, J. W. Fraser, G. Champion, and H. J. Labbe, *J. Electrochem. Soc.*, **146**, 735 (1999).
66. N. Quill, I. Clancy, S. Nakahara, S. Belochapkine, C. O'Dwyer, D. N. Buckley, and R. P. Lynch, *ECS Trans.*, **77**, 67 (2017).
67. R. J. Gilliam, J. W. Graydon, D. W. Kirk, and S. J. Thorpe, *Int. J. Hydrogen Energ.*, **32**, 359 (2007).